COOPERATIVE H_2 ACTIVATION AT A NICKEL(0)-OLEFIN CENTER

María L. G. Sansores-Paredes,[1] Martin Lutz[2] and Marc-Etienne Moret.[1]

[1]Organic Chemistry and Catalysis, Institute for Sustainable and Circular Chemistry, Faculty of Science. Utrecht University. Universiteitsweg 99, 3584 CG, Utrecht, The Netherlands.
Email: m.moret@uu.nl
[2]Structural Biochemistry, Bijvoet Centre for Biomolecular Research, Faculty of Science. Utrecht University, Universiteitsweg 99, 3539 CG, Utrecht, The Netherlands.

ABSTRACT

Catalytic olefin hydrogenation reactions are ubiquitous in organic synthesis. Most proposed catalytic cycles for the homogeneous hydrogenation of olefins using molecular H_2 start with the oxidative addition of H_2 by metal complexes to form two reactive M–H bonds, often via a non-classical metal dihydrogen (M–H_2) intermediate. Previous reports had provided indirect evidence for an alternative mechanism involving direct hydrogen transfer from a metal-bound H_2 molecule to a metal-bound olefin without the oxidative addition step. However, the key metal(olefin)(H_2) and the corresponding ligand-to-ligand hydrogen transfer (LLHT) step had not been directly observed. Herein, we show that incorporating a precoordinated olefin in a P(C=C)P pincer ligand framework allows for the observation of both a non-classical Ni-(H_2) complex and the Ni(alkyl)(hydrido) product of LLHT in rapid equilibrium with dissolved H_2. The utility of this cooperative H_2-activation mechanism for catalysis is demonstrated in the semihydrogenation of diphenylacetylene under mild conditions. Mechanistic investigations supported by DFT calculations back the central role of LLHT for both cooperative H_2 activation and catalytic semihydrogenation. These results provide an experimental basis for the role of LLHT steps in olefin hydrogenation mechanisms and demonstrate the utility of olefin-based pincer ligands for cooperative catalysis with non-noble metals.

INTRODUCTION

Catalytic hydrogenation reactions are ubiquitous in the industrial synthesis of both bulk and fine chemicals.[1–3] The addition of H_2 to a substrate molecule is atom economic and generally cost-effective, making such reactions very attractive from an environmental point of view.[2–6] This prospect has motivated a continuous effort towards understanding the activation of H_2 by transition metal catalysts. Classically, reduced transition metal centers activate the H–H bond via two bonding interactions (Figure 1, a): σ-donation by the H_2 ligand to a metal vacant site and π-backdonation from the metal d-electrons to the σ^*(H–H) orbital. Strong orbital interactions result in oxidative addition, fully cleaving the H–H bond to form a metal dihydride (Figure 1, b).[3,4,6–8] In contrast, weaker interactions result in non-classical dihydrogen complexes, in which some extent of H–H bonding is preserved.[8–10]

Activation of molecular H_2 with 3d metals is generally more challenging than with 4d or 5d metals because they tend to form weaker M–H bonds. Nevertheless, the use of 3d metals for hydrogenation reactions has attracted considerable interest in view of their abundance, low cost, and generally lower toxicity.[11] Bifunctional catalysts that rely on ligands actively participating in the cleavage of the H–H bond[11–14] play a central role in this transition (Figure 1, c).[11–13,15–19] In particular, Lewis bases incorporated in the ligand can accept a proton from the H_2 molecule to generate a hydride.[11,13,20–23] A related, very successful strategy relies on reversible

aromatization/dearomatization of a N-heterocyclic ligand.[17] In both of these processes, the formal oxidation state of the metal remains unchanged. More recently, Lewis acids have been found able to accept a formal hydride from H_2 to form a M–H bond with concomitant oxidation of the metal.[11,13,20–23] Additionally, bimetallic systems have been successfully applied, in which metal-metal proximity helps polarizing and cleaving the H–H bond.[13,24]

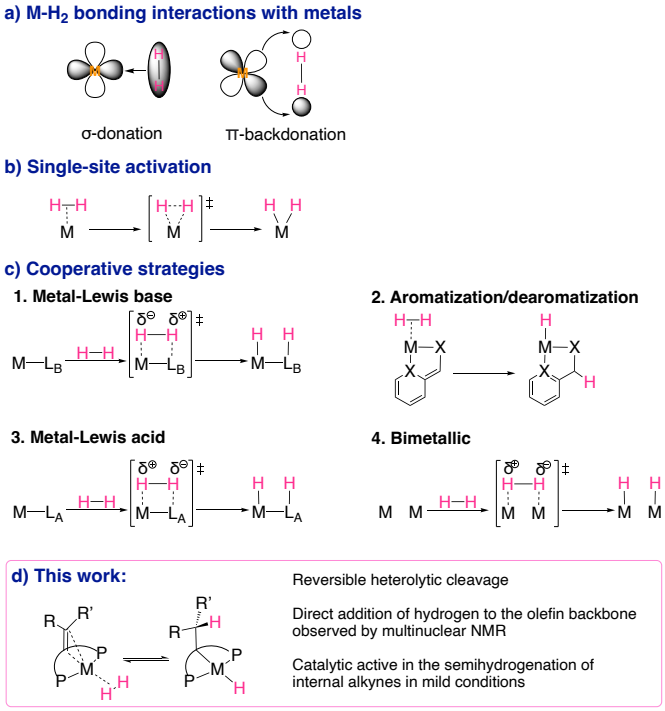

Figure 1. Strategies of H_2 activation in homogeneous catalysis.

Against this backdrop, we hypothesized that a π-bound olefin could be used as an element of ligand design for H_2 activation. Since the discovery of non-classical H_2 complexes by Kubas,[25] knowing whether they can transfer hydrogen atoms to unsaturated substrates *without prior H–H cleavage* has been a long-standing question. Supporting evidence came, amongst other, from kinetic studies on olefin hydrogenation involving a diruthenium-H_2 intermediate and parahydrogen induced polarization (PHIP) experiments on photoinduced hydrogenation mediated by transient $[Mo(CO)_3(H_2)(olefin)]$.[3,26–31] A few examples of metal complexes bearing a PC=CP pincer ligands have been reported; one example undergoing reversible interconversion between an olefin metal hydride and the corresponding metal-alkyl formed by β-insertion, showing that hydride migration can occur between ligands occupying *trans* positions.[15,32–39] The fact that alkyl complexes of 3d metals such as Ni(II) are often thermodynamically resistant to β-hydride elimination further suggested that hydride transfer to a bound olefin could provide the much-needed driving force for cooperative H_2 activation.[40] Additionally, the hydricity of the resulting Ni–H bond may be enhanced by the trans alkyl carbon.[41,42] Therefore, we set out to investigate the ability of Ni(0) complexes of PC=CP pincer ligands to activate and transfer H_2.

In this report, we show that the incorporation of a precoordinated olefin in a pincer ligand framework allows for the observation of both a non-classical Ni-(H_2) intermediate and the corresponding alkyl(hydrido) activation product, both in rapid equilibrium with dissolved H_2. Experiments and DFT calculations support a direct ligand-to-ligand hydrogen transfer (LLHT) mechanism without a dihydride intermediate. The catalytic relevance of this cooperative mechanism is demonstrated in the selective semihydrogenation of diphenylacetylene to Z-

stilbene under mild conditions, with a comparable performance to recently disclosed Ni-based systems.[5,43–47]

RESULTS AND DISCUSSION

Hydrogen activation. We had previously reported the synthesis of a Ni(0)-N_2 complex of the bulky olefin pincer ligand ^{Ph}bppe^{H,CHptol2} by ring-opening of the corresponding nickelacyclobutane.[48] In the solid state, the complex had been characterized as the N_2–bridged dimer [(^{Ph}bppe^{H,CHptol2})Ni]$_2$(μ-N_2) (1^{dimer}, Figure 2). In toluene solution under N_2, an intense IR absorption at 2150 cm^{-1} indicates the presence of the mononuclear form (^{Ph}bppe^{H,CHptol2})Ni(N_2) (**1,** Figure 2; see also SI section 2).[48,49] The N_2 coligand was easily displaced by addition of H_2 (1 atm) to a solution of complex **1** in d^8-tol. At 25 ºC, both ^{31}P{^{1}H} and ^{1}H NMR spectra displayed broad signals. Intriguingly, the expected signal of dissolved H_2 was absent from the ^{1}H NMR spectra, suggesting exchange processes involving H_2.[23] Cooling the solution down to –40 ºC caused the reappearance of the H_2 signal at 4.54 ppm and decoalescence of both ^{31}P{^{1}H} and ^{1}H NMR spectra to sharp lines, allowing for the identification of three Ni-containing species (Figure 2, a. See SI sections 1.1 and 1.2).

Two minor species are observed: the first one is a residual amount of the known N_2 complex **1** as shown by two ^{31}P NMR doublets at 11.3 and 28.2 ppm ($J_{P,P}$= 53 Hz) and an ^{1}H NMR signal at δ 4.75 ppm corresponding to the olefinic CH group. The second minor species displays similar characteristics: two ^{31}P NMR doublets at 15.5 and 32.8 ppm ($J_{P,P}$= 58 Hz) and an olefinic ^{1}H signal at δ= 4.35 ppm that was shown to couple with the ^{31}P NMR signal at 15.5 ppm by ^{1}H-^{31}P HMBC (see SI section 1.1). It also features a broad ^{1}H NMR signal at –2.1 ppm which suggested its assignment as the nonclassical-H_2/olefin species **2.** This was unambiguously confirmed by repeating the experiment under an HD atmosphere, which resulted in the appearance of a triplet signal (Figure 2, b) with a $^1J_{H,D}$ coupling constant of 34 Hz, corresponding to a H–H bond length of 0.86 Å according to the Heinekey empirical relationship.[2,4,50,51] The value corresponds to a true dihydrogen complex and is in good agreement with previous reports for Ni(0)–H_2 complexes.[2,4,20,23,44,50–53]

The major species was assigned as the alkyl(hydrido) Ni(II) complex **3** resulting from cooperative H_2 addition concomitantly forming new C–H and Ni–H bonds. A single, slightly broadened ^{31}P signal at 40.6 ppm (see SI 1.1) indicates two chemically equivalent P atoms. In the ^{1}H NMR spectrum, (Figure 2, b), a triplet signal at δ –14.3 ppm ($^2J_{H,P}$= 54 Hz) evidences a Ni–H bond with coupling to two equivalent phosphorus nuclei. A slightly broadened signal at δ 3.1 ppm corresponds to the alkyl CH_2 group, as also supported by a long-distance J-coupling with the Ni–H signal observed by ^{1}H-^{1}H COSY (see SI 1.1). The alkyl CH group appears as a triplet signal at δ 3.8 ppm ($^3J_{H,H}$= 8.4 Hz) due to coupling with the two equivalent hydrogen atoms of the CH_2 group. Peak assignment was corroborated by an APT ^{13}C experiment (see SI section 1.1).

An ^{1}H-^{1}H EXSY experiment at –40ºC confirmed rapid chemical exchange between complex **2**, complex **3** and dissolved H_2 (Figure 2, c). Namely, cross-peaks were observed between the Ni–H signal of **3** at –14.3 ppm and free H_2 (4.54 ppm), the Ni–H_2 signal of **2** at –2.1 ppm, and the CH_2 signal of **3**. In addition, exchange between free and Ni-bound H_2 was also observed. These observations support facile and reversible transfer of a hydrogen atom from an Ni-bound H_2 to an Ni-bound olefin with no detectable dihydride intermediate.

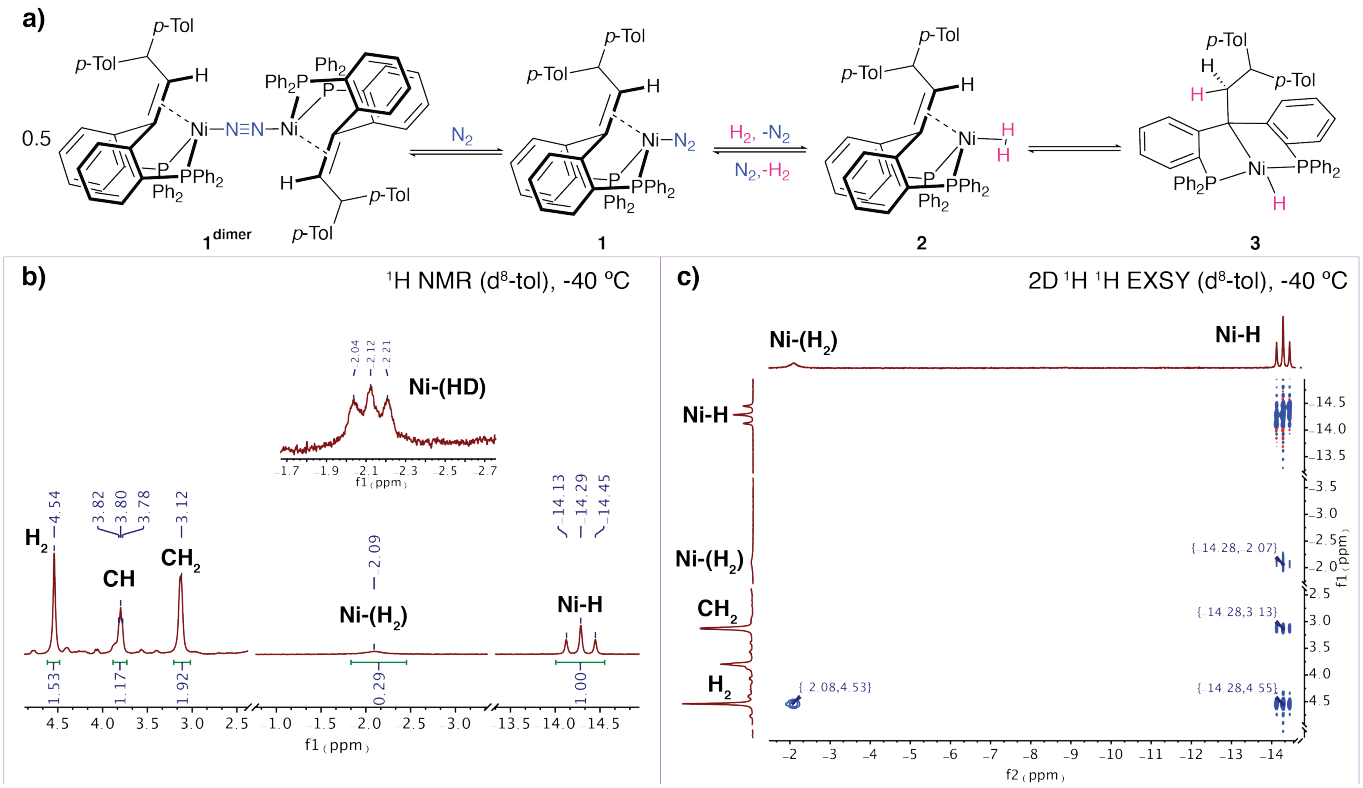

Figure 2. a) Equilibrium among complex **1**^{dimer}, **1**, **2** and **3** under H_2 atmosphere. b) Bottom: extract of an ^1H NMR spectrum at -40 ºC in d^8-tol of the equilibrium among **1**,**2** and **3**. On top: Extract of $^1H\{^{31}P\}$ NMR at -40 C in d^8-tol depicting the Ni-(HD) peak under HD atmosphere (see SI section 2.1). c) Extract of the 2D 1H-1H EXSY spectrum at -40 ºC in d^8-tol of the equilibrium among **1**,**2** and **3** (see SI section 2.2).

DFT calculations support a concerted activation pathway (Figure 3, a). Exchange of N_2 for H_2 to form the non-classical Ni–H_2 complex **2** from complex **1** is slightly endergonic (7.5 kcal/mol). A concerted transition state for H_2 activation, **TS1**, was located 13.3 kcal/mol above complex **2** and is directly connected to structure **3a,** a higher energy rotamer of the final alkyl(hydrido)nickel complex **3.** The total exergonicity of –8.4 kcal/mol from **2** to **3** is consistent with **3** being the main species in solution but slightly overestimated. A putative nickel-dihydride structure was also located at 15.1 kcal/mol. However, forming this structure requires the olefin to leave the coordination sphere of Ni and no transition state connecting it to the products could be located. (see SI section 4.4).

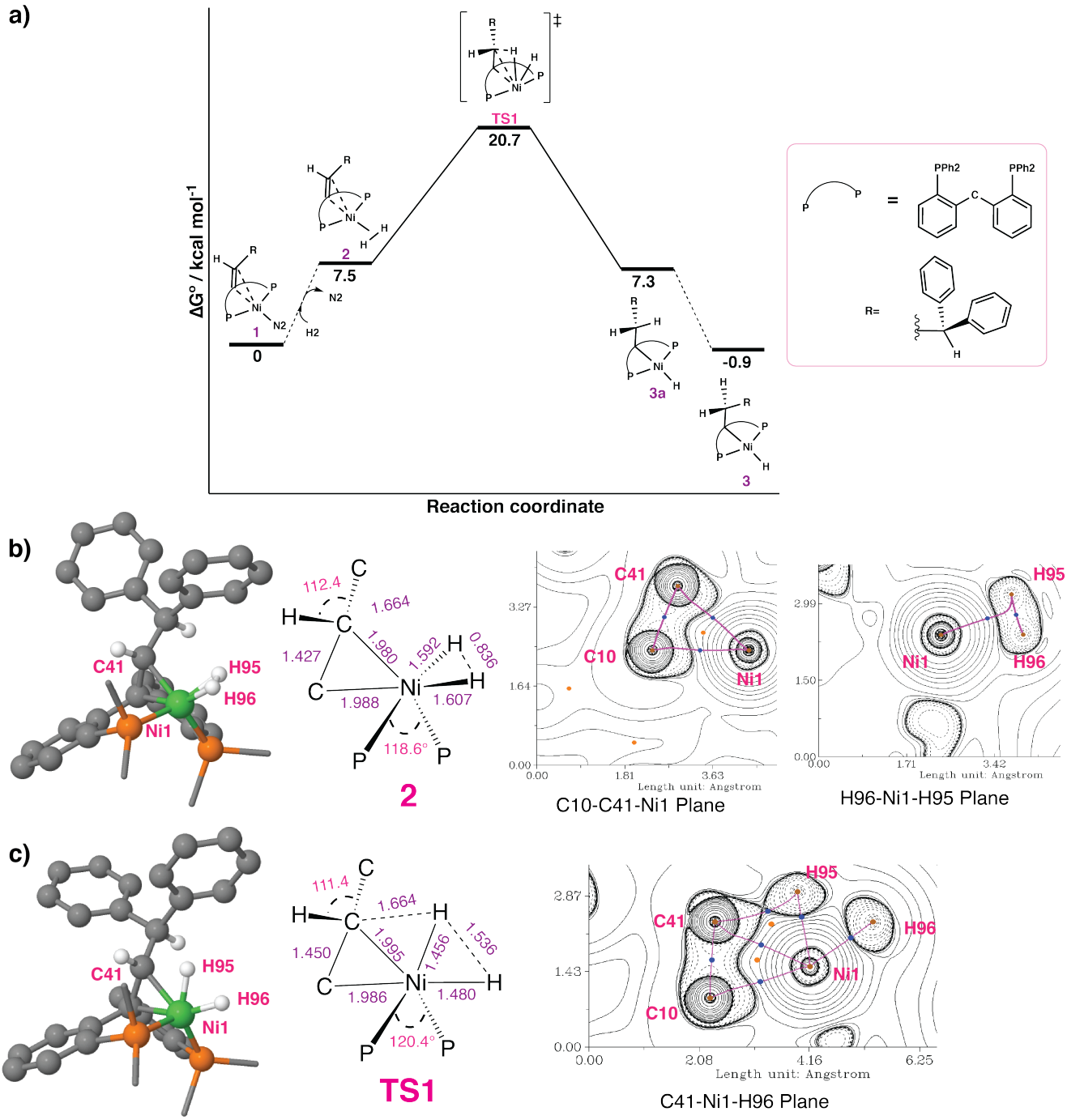

Figure 3. a) Gibbs free energy profiles for H_2 activation computed at the B3LYP-GD3BJ/def2TZV/SMD//B3LYP-GD3BJ/6-31(d,p) level of theory using toluene as solvent. Dotted lines mark pathways for which no transition state was computed. b) on the left: relevant distances and angles of the optimized structure of complex **2**. On the right: two views of the Laplacian map with the positive area (ionic bond area; solid lines) and negative area (covalent bond area; dashed lines) from the QTAIM topological analysis of complex **2**. Electron density was extracted from a single-point calculation at the B3LYP-GD3BJ/def2TZVP level of theory on the optimized geometry computed at B3LYP-GD3BJ/6-31(d,p) level of theory. Blue dots represent BCP and orange points RCP. c) On the left: relevant distances and angles of Transition state 1 (TS1). On the right: the Laplacian map with the positive area (ionic bond area; solid lines) and negative area (covalent bond area; dashed lines) from the QTAIM topological analysis of TS1. Electron density was extracted from a single-point calculation at the B3LYP-GD3BJ/def2TZVP level of theory on the optimized geometry computed at B3LYP-GD3BJ/6-31(d,p) level of theory. Blue dots represent BCP and orange points RCP.

The optimized structure of complex **2** (Figure 3, b) confirms its assignment as a genuine H_2 complex with an H–H bond length is 0.836 Å, in good agreement with the experimental estimation (0.86 Å).[2,4,50,51] The C=C backbone is slightly elongated (1.427 Å) as consequence of π-backdonation from the nickel center and exhibits a sum of valence angles of 354.4º and 351.6º around C10 and C41, respectively. Interestingly, the H–H vector is out of the Ni-olefin plane, suggesting that both ligands are receiving π-backdonation from different d-orbitals. Well-characterized Ni(0)–H_2 complexes were hitherto limited to those incorporating an additional σ-ligand[54] or a σ-acceptor, Z-type ligand. Such ligands can assist coordination by lowering the energy of the σ-antibonding d-orbital[2,4,6,20,23,49,53,55–57] and, in some cases, allow H_2 deprotonation to form strongly hydridic d^{10} hydrides.[58,59] The observation of complex **2** demonstrates that a single π-acidic olefin ligand is sufficient to stabilize a H_2 complex of a d^{10} metal and can cooperatively generate an active hydride without the need for full oxidative addition to a dihydride intermediate, warranting consideration of such pathways in catalytic hydrogenation reactions.

The structure of **TS1** is particularly interesting in view of the cooperative role of the olefin ligand (Figure 3, c). In **TS1**, H_2 undergoes a formal heterolytic cleavage where the olefin is reduced by accepting a hydride equivalent and the nickel center accepts a proton, increasing its oxidation state by two units. The carbon atoms belonging to the olefin (C10 and C41) maintain close to sp^2 character with a bond length of 1.450 Å and sum angles of 348.0º and 352.8º respectively. The fragment is still coordinated in η^2 fashion to the nickel center with similar bond length values than in complex **2**. The H–H bond is broken with a distance of 1.536 Å and, both the Ni–H95 (1.456 Å) and Ni–H96 (1.480 Å) distances have become shorter than in structure **2**. These structural observations collectively suggest that the transition state has a strong dihydride character, the metal being already oxidized to Ni(II).

To shed more light onto the hydrogen transfer mechanism, a QTAIM analysis[60,61] of **2** and **TS1** was performed. QTAIM analysis of complex **2** (Figure 3, b) showed bond critical points (BCP) from both carbons of the olefin and nickel located in the ionic area and the BCP of the olefin in the covalent area (C41–Ni1 $\nabla\rho^2$= 0.250, C10–Ni1 $\nabla\rho^2$= 0.237 and C41–C10 $\nabla\rho^2$= -0.753), as typical for metal olefin complexes. The interaction with nickel and H_2 shows a bond path that originates from the nickel atom towards the center of the H–H bond, but curves towards one of the hydrogen atoms (Ni1–H95 $\nabla\rho^2$= 0.395). This can be explained as a “bond catastrophe”: the BCP in between Ni–H96 and the RCP for Ni–H95–H96 have coalesced, as has been observed before in the analysis of other non-classical dihydrogen complexes and olefins.[62,63] QTAIM analysis of **TS1** present interesting features (Figure 3, c). The Ni-bound olefinic backbone displays similar BCP characteristic values to complex **2** (C41–Ni1 $\nabla\rho^2$= 0.259 and C10–Ni1 $\nabla\rho^2$= 0.242 and C41–C10 $\nabla\rho^2$= –0.707). The H–H bond is broken, but both atoms are bonded to nickel. Both interactions with nickel are ionic with a slight difference between them (Ni–H95 $\nabla\rho^2$= 0.121 and Ni–H96 $\nabla\rho^2$=0.084) but a significant increase in covalency with respect to the Ni–H_2 interaction in complex **2**. A BCP between C41 and H95 located in the ionic area ($\nabla\rho^2$= 0.010) corresponds to the barely formed C–H bond. These observations support the description of **TS1** as resembling an olefin-bound Ni(II) dihydride (NiH_2) complex.

This description of **TS1** is consistent with a ligand-to-ligand hydrogen transfer mechanism (LLHT)[61,64,65] consisting of a concerted hydrogen atom transfer between two ligands (the H_2 molecule and the olefin) with concomitant oxidation of nickel. This mechanism was first described for the Ni-catalyzed hydrofluoroarylation of alkynes: a fluoroarene first coordinates in η^2(C,H) fashion to an η^2(C,C)-alkyne nickel(0) complex to then transfer an H atom to the alkyne without a hydride intermediate, generating an agostic vinyl group. This mechanism is favored for metals with a small radius such as nickel and LLHT steps have been invoked for C–H bond activation reactions at nickel/olefin complexes.[61,64–70]. Alternatively, **TS1** could be viewed as a σ-CAM type

mechanism if the olefin adduct is described as the nickelacyclopropane extreme of the DCD model. In that case the oxidation state of Ni(II) does not change and the transfer occurs between σ-bonds.

Catalytic activity in the semihydrogenation of alkynes. Having found that complex **1** activate H_2 efficiently and reversibly, we investigated the applicability of H_2 activation by LLHT in catalytic hydrogenation. Inspired by recent progress in the nickel-catalyzed semihydrogenation of internal alkynes using H_2 as hydrogen source,[5,43–45] we chose the hydrogenation of diphenylacetylene as model reaction. With 10 mol% catalyst at 70 °C in d^8-tol under 4.6 atm H_2 after 22 hours, E-stilbene (80 %) and Z- stilbene (12 %) with a small amount of overhydrogenation to diphenylethane (8 %) were detected. The solution remained visually homogeneous throughout the reaction, and a mercury drop did not hinder catalysis, suggesting a homogeneous system. Gradually decreasing the catalyst loading to 1 mol% still allows full conversion to mostly stilbenes, albeit with a longer reaction time at 1 mol%. Intriguingly, the Z:E ratio markedly changes from 12:80 to 88:9 with decreasing catalyst loading.

Table 1. Product ratio in the semihydrogenation of diphenylacetylene for different catalyst loadings

Cat. Loading (%)	Time (h)	Z-stilbene (%)	E-stilbene (%)	Diphenylethane (%)	Conversion (%)
1	43	88	9	1	98
2.5	24	51	44	5	>99
5	20	26	70	4	>99
10	22	12	80	8	>99

Reaction conditions: J-Young NMR tube, precatalyst = complex 1, 70 °C oil bath, volume 0.55 mL of d^8-tol, conversion and products were monitored by ^{1}H-NMR using mesitylene as internal standard.

To get more insight into this dependency and into the reaction mechanism in general, we monitored the reaction with 10 mol% catalyst loading by ^{1}H NMR (Figure 4), which revealed two well-separated regimes. First, as long as diphenylacetylene is present in excess of the catalyst, clean conversion to Z–stilbene occurs with an apparent zero order with respect to diphenylacetylene (Figure 4, a). Then, rapid isomerization of Z-stilbene to E-stilbene starts taking place reaching a Z:E ratio of 6:3. After a short period of time (ca. 1h), the process considerably slows down and does not reach thermodynamical equilibrium. Concomitantly, small amounts of the overhydrogenation product diphenylethane are formed. To rule out simultaneous semihydrogenation and isomerization, a substrate competition experiment was performed using equal amounts of diphenylacetylene and Z-stilbene at the beginning of the reaction with 10 % mol catalyst. The results showed that semihydrogenation takes place first and after isomerization of stilbene (see SI section 1.3).

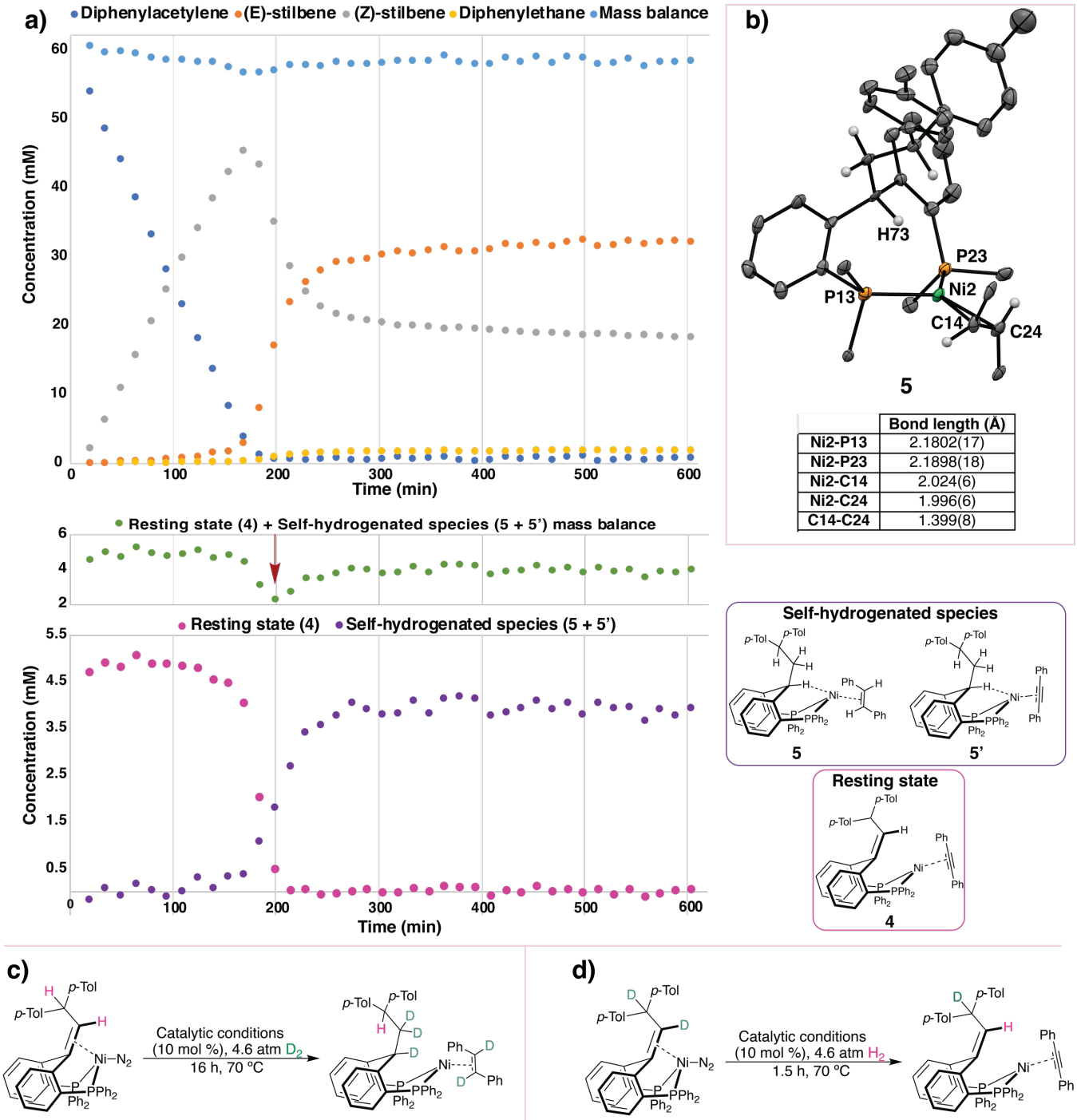

Figure 4. Kinetic profiles of semihydrogenation of diphenylacetylene at 70 °C in d8-tol at 10% mol catalyst and related experiments. Concentrations were determined by ^{1}H NMR using mesitylene as internal standard. A) On top, kinetic profile at 10 % mol catalyst loading at 70 °C heated and monitored by ^{1}H NMR. Bottom: profile of detected catalyst speciation during semihydrogenation of diphenylacetylene (resting state **4** and self-hydrogenated species **5** and **5'**). The green dots represent the total concentration of detected species plotted in a separate graphic for clarity. The red arrow marks a temporary decrease in the total concentration of detected species, suggesting a buildup of the hydride mixture **2** ⇄ **3** that cannot be detected under these conditions because it gives broad features. B) Molecular structure of self-hydrogenated product **5** determined by X-ray crystallography with selected bond lengths.[72] Only one of two independent molecules is shown. Hexane solvent molecules and the phenyl groups of the phosphines and of the (E)-stilbene coligand are omitted for clarity. c) Formation of partially deuterated self-hydrogenated species **5** in catalytic conditions under D_2 atmosphere. d) Deuterium scrambling of d2-complex **1** in catalytic conditions under H_2 atmosphere.

The transition between those two regimes is accompanied by a change in catalyst speciation evidenced by *operando* ^{1}H NMR and ^{31}P NMR data. In the first regime, the only observable Ni-containing species is the diphenylacetylene π-complex **4** (Figure 4, a), which also could be independently prepared by treating complex **1** with equivalent of diphenylacetylene. An olefinic ^{1}H signal at ∂ 5.72 ppm indicates that the olefin backbone decoordinates from Ni when the π-acidic alkyne binds, as has been observed for a related ketone pincer ligand (see SI section 2).[71] Once diphenylacetylene has been consumed, complex **4** gradually disappears, which coincides with the onset of (E)-(Z) isomerization and overhydrogenation. At this time, a temporary decrease is observed in the total concentration of detected Ni species: the hydride mixture **2** ⇄ **3** likely accumulates in the reaction medium, but it cannot be detected at these concentrations because it gives broad signals (see Figure 4, a. Catalyst mass balance, red arrow). Supporting this idea, neither (Z)- nor (E)-stilbene displaced the N_2 ligand in **1** in stoichiometric experiments**,** showing that these olefins cannot occupy the same binding site as diphenylacetylene in **4** (see SI section 1.4). In the same time period, two new complexes gradually appear. The main species could be isolated after reaction and identified both spectroscopically and crystallographically as the E-stilbene complex **5** (see Figure 4, b), in which the olefin backbone has been hydrogenated (self-hydrogenation).[72] In C_6D_6 solution, it displays a characteristic deshielded aliphatic multiplet ^{1}H signal at ∂ 8.38-8.52 ppm corresponding to the central C–H unit engaging in an anagostic interaction with the nickel center (H73).[73] The minor species was identified *in situ* as the self-hydrogenated complex but with diphenylacetylene as coligand, **5'** (see SI sections 1.3, 1.5). When **5** and **5'** reach their final concentration, overhydrogenation stops and (E)-(Z) isomerization becomes exceedingly slow, suggesting that catalyst self-hydrogenation shuts down both pathways. Indeed, the isolated complex **5** revealed a sluggish isomerization catalyst under relevant conditions (10 mol%, 70ºC, 4.6 atm H_2): after 24h, the isomerization reaction has not completed (~20 %) and only trace amounts of diphenylethane are observed. Complex **5** is also inactive for the hydrogenation of diphenylacetylene when only ligand exchange between diphenylacetylene and (E)-stilbene is observed (see SI section 1.5).

To assess whether the allylic H atom of the olefin pincer ligand participates in the catalytic reaction, we resorted to isotope labeling experiments. Performing the hydrogenation with D_2 expectedly results in rapid deuteration of the olefinic proton of **4,** but no deuterium incorporation at the allylic C–H position is observed (Figure 4, c). The experiment using a complex **1** deuterated in alkyl and olefinic positions results in scrambling of hydrogen uniquely in the olefin position (Figure 4, d). These experiments rule out any direct involvement of this allylic position in the hydrogenation mechanism (see SI section 1.4)

The observations above suggest that the final product distribution is largely determined by the competition between (E)-(Z) isomerization and catalyst self-hydrogenation. This competition could be studied separately by exposing (Z)-stilbene to **1** (10 mol %) under an H_2 atmosphere at 70ºC (see SI 1.3). At early times, rapid catalytic isomerization to (E)-stilbene was observed together with gradual appearance of the self-hydrogenation product **5**; the ^{1}H NMR signal of free H_2 was broad, suggesting the presence of hydride mixture **2** ⇄ **3** in addition to complex **5.** After ca. 2h (ca. 77% conversion), isomerization considerably slowed down, the ^{1}H NMR signal of H_2 became sharp, and complex **5** was still the only Ni-containing species detected by ^{1}H NMR. A maximum of 82 % conversion (incl. 2 % diphenylethane) was reached after 10h. In contrast, no isomerization was observed under an N_2 atmosphere, showing that complex **1** alone is inactive. These results confirm that the hydride mixture **2** ⇄ **3** generated from **1** under H_2 catalyzes olefin isomerization, presumably via a hydride mechanism, and decays to complex **5** by self-hydrogenation. Interestingly, the same reaction at 25 ºC reached 93 % conversion to E-stilbene

after 10h with barely any overhydrogenation (1%), suggesting that temperature can be used to control the relative rates of self-hydrogenation *vs.* catalytic isomerization.
While the self-hydrogenation process forming the inactive complex **5** could formally be initiated by C–H reductive elimination from hydride **3**, such a reaction is unlikely for *trans* substituents in a square-planar structure.[41] Accordingly, heating either **1** or its benzonitrile analogue[48] (benzonitrile is a weaker ligand than phenylacetylene) under an H_2 atmosphere does not result in any observable C–H bond formation (see SI section 1.4). In contrast, the clean formation of complex **5** from **1** and H_2 in the presence of (E)- or (Z)- stilbene suggests that an olefin acting as a "hydride shuttle" takes part in this process.

DFT calculations performed on a slightly truncated model support the mechanistic scenario outlined in Figure 5 (details in SI section 4), which accounts for the experimental observations. The semihydrogenation cycle starts with the endergonic (+16.7 kcal/mol) displacement of diphenylacetylene for H_2 to form complex **2** from resting state **4**. Rate-limiting H_2 cleavage via LLHT (see above) yields complex **3** with an overall activation energy of 29.9 kcal/mol, consistent with a slow reaction at 70 °C.[74] Endergonic coordination of diphenylacetylene yields complex **6**, followed by insertion ($\Delta G^{\ddagger}$ = 25.8 kcal/mol) to form the vinyl complex **7**. To complete the catalytic cycle, transfer of a hydrogen atom from the CH_2 backbone to the vinyl ligand forms Z-stilbene and regenerates the olefin backbone with an overall barrier of 30.9 kcal/mol. Interestingly, two nearly isoenergetic pathways were identified for the C–H formation step: a stepwise β-hydride elimination/reductive elimination sequence involving a high-lying nickel hydride or a concerted LLHT-like step akin to that found for H–H cleavage (details in SI section 4.1).[61,65] The associated barriers are ca. 1 kcal/mol higher than that for H_2 cleavage, but this step will be additionally favored by concentration effects in the presence of an excess of alkyne substrate. A σ-bond metathesis pathway cleaving the Ni–C bond of complex **7** with an incoming H_2 molecule to form **3** directly was also considered but was found energetically inaccessible with an overall barrier of 38.7 Kcal/mol (see SI section 4.5).

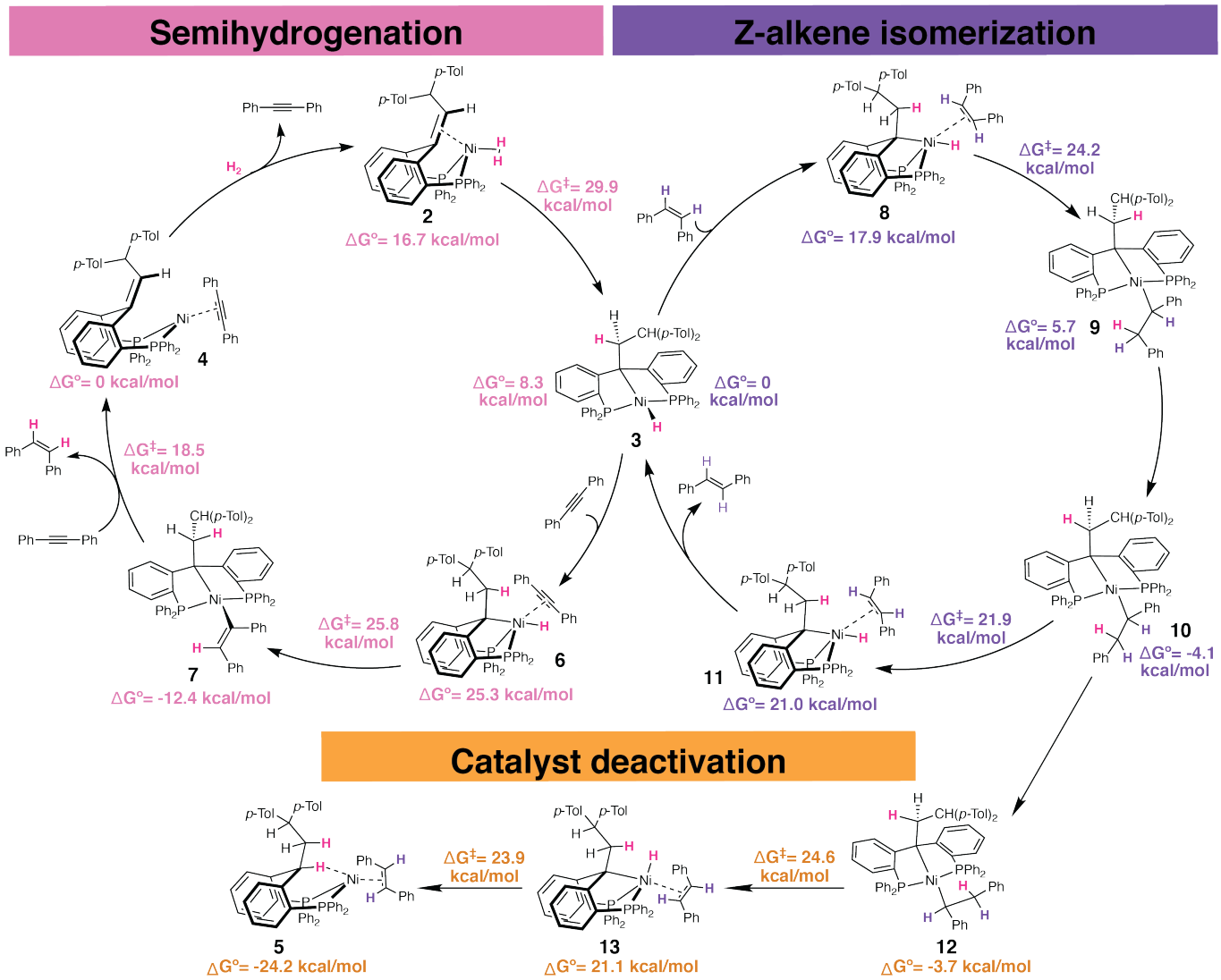

Figure 5. Computed catalytic cycles for semihydrogenation of diphenylacetylene and Z-stilbene isomerization, and computed pathway for the formation of complex **5.** Gibbs free energies for intermediates and transition states were calculated at the B3LYP-GD3BJ/def2TZV/SMD//B3LYP-GD3BJ/6-31(d,p) level using toluene as solvent. In the calculations, the tolyl groups were substituted by phenyl groups, but the tolyl groups are plotted in the figure for clarity.

Once diphenylacetylene has been consumed, the isomerization catalytic cycle starts. In agreement with experiment, the associated barriers would be prohibitively high (32.5 kcal/mol) with the diphenylacetylene complex **4** as resting state but become readily accessible when the hydride compound **3** can accumulate in solution. Endergonic (17.9 kcal/mol) coordination of Z-stilbene to hydride complex **3** to form complex **8** is followed by hydride insertion ($\Delta G^{\ddagger}$ = 24.2 kcal/mol) yielding *trans*-dialkyl nickel complex **9**. Facile C–C bond rotation to form conformer **10** followed by β-hydride elimination ($\Delta G^{\ddagger}$= 21.9 kcal/mol) releasing E-stilbene to regenerate **3** complete the isomerization cycle (details in SI 4.2).

Because the catalyst deactivation is in competition with the isomerization process according to the experimental data, we also investigated its mechanism. A possible pathway starts with the rotation of the Ni–C bond of complex **10** to yield conformer **12** (–3.7 kcal/mol). β-hydride elimination ($\Delta G^{\ddagger}$ = 24.6 kcal/mol) takes place yielding complex **13** that subsequently undergoes reductive elimination resulting in complex **5**. Another possible pathway involves a concerted hydrogen transfer transition state: a hydrogen atom is transferred from one alkyl ligand to the alkyl

ligand part of the pincer backbone in complex **12** with energy barrier of $\Delta G^{\ddagger}$= 25.0 kcal/mol yielding complex **5** (see SI 4.6). The overall barrier for self-hydrogenation is slightly higher than the isomerization process (2.7 Kcal/mol), consistent with the catalyst performing a few isomerization turnovers before decaying *via* the thermodynamically favored self-hydrogenation pathway. Other pathways considered were the reductive elimination from hydrides **3, 8** or **11**, which were all prohibitively high in energy, in accord with the difficulty of such a process for *trans* substituents in a square-planar structure. Concerted hydrogen transfer from complex **10** (no rotation) were also not feasible to yield complex **5** (see SI 4.6).

CONCLUSION

In summary, we describe the cooperative activation of molecular H_2 by a nickel-olefin complex. Incorporating a precoordinated olefin in a pincer ligand framework allowed for the direct observation of a rapid chemical exchange between free H_2, a non-classical (olefin)Ni-(H_2) complex, and an alkyl(hydrido) nickel(II) species by NMR spectroscopy. Experimental observations and DFT calculations support a Ligand-to-Ligand Hydrogen Transfer (LLHT) mechanism, that is a concerted H atom transfer from the metal-coordinated H_2 molecule to the olefin without prior oxidative addition of H_2. The reported system is an active catalyst for the semihydrogenation of diphenylacetylene using molecular H_2. Mechanistic investigations and DFT studies illustrate the importance of LLHT steps for nickel, which contrasts with heavier group 10 elements.

These results provide an experimental basis for considering LLHT steps in olefin hydrogenation mechanisms, especially with catalysts based on first-row transition metals. Furthermore, they demonstrate the potential of a tethered C=C double bond in the cooperative activation of small molecules, opening a new avenue for the design of environment-friendly cooperative catalysts using non-noble metals. Further applications of this concept are currently investigated in our laboratory.

ACKNOWLEDGEMENTS

This project has received funding from the European Research Council (ERC) under the European Union's Horizon 2020 research and innovation program (grant agreement No. 715060). The X-ray diffractometer has been financed by the Netherlands Organization for Scientific Research (NWO). The computational work was carried out on the Dutch national e-infrastructure with the support of the SURF Foundation. We thank Dr. P. M. Pérez-García for his assistance with the analysis of the catalysis results and helpful discussion. We thank Prof. G. van Koten, Prof. W. Hill Harman, Dr. D. L. J. Broere and Dr. A. A. Thevenon-Kozub for insightful discussions.

AUTHOR CONTRIBUTIONS

Dr. M.-E. Moret initiated and supervised the project. M. L. G. Sansores-Paredes performed the experiments and DFT calculations. Dr. M. Lutz oversaw the acquisition, solving and interpretation of X-ray diffraction of the crystal structure. M. L. G. Sansores-Paredes and Dr. M.-E. Moret wrote the manuscript with the contribution of Dr. M. Lutz. All authors approved the final manuscript.

METHODS

General information: All reactants were purchased from commercial sources and used as received without further purification unless otherwise noted. (E)-stilbene, (Z)-stilbene and

diphenylacetylene were stored in the glovebox. Additionally, (Z)-stilbene and mesitylene were degassed by three freeze-pump-thaw cycles before use.
All the reactions were performed under an N_2(g) atmosphere in the glovebox. Deuterated solvents were purchased from Cambridge Isotope Laboratory Inc. (Cambridge, USA), degassed by three freeze-pump-thaw cycles, and stored over molecular sieves before use. Common solvents were dried using a MBRAUN MB SPS-80 purification system and/or distillation technique. [(^{Ph}bppe^{H,CHptol2})Ni]N_2 was synthetized according to literature procedure.[48]

Physical methods: ^{1}H, ^{13}C and ^{31}P NMR spectra (400, 100, 376 and 161 MHz respectively) were recorded on an Agilent MR400 or a Varian AS400 spectrometer at 297 K unless it is stated differently. ^{1}H and ^{13}C NMR chemical shifts relative to tetramethylsilane are referenced to the residual solvent resonance unless stated otherwise. Infrared spectra were recorded using a Perking Elmer Spectrum One FT-IR spectrometer under N_2 flow. GC analyses were performed on a Perkin-Elmer Clarus 500 GC [column PE, Elite-5, 30m x 0.32 mm x 0.25 μm, (5% phenyl)-(95% methyl)polysiloxane)] and a flame-ionization detector (FID).

General catalysis procedure: Stock solutions of catalyst (0.012 M) and diphenylacetylene (0.1 M) in deuterated toluene were prepared in the glovebox. In a vial, 0.25 mL of catalyst solution and 0.3 mL of diphenylacetylene solution were added turning the solution red. With a microsyringe, 4.2 μL of mesitylene were added to the solution and mixed. The reaction mixture was transferred to a J-Young NMR tube. The tube was connected to a gas setup and degassed by two freeze-pump-thaw cycles and with the solution inside of a Dewar with liquid nitrogen, hydrogen gas was introduced. The solution was warmed up at room temperature and analyzed and placed in an oil bath at 70 ºC. The concentrations of products were determined by ^{1}H NMR using mesitylene as internal standard. Proton peaks used in quantification (d^8-tol, 400 MHz):[44] Diphenylacetylene: 7.46 (m, 4H)
(E)-stilbene: 7.29 (dd, *J*= 8.3, 1.3 Hz, 4H)
(Z)-stilbene: 6.44 (s, 2H)
1,2-diphenylethane: 2.72 (s, 1H)
Mesitylene: 6.67 (s, 3H)

Mercury drop experiment procedure: Two Schlenk bombs with stirring bars (one containing a drop of mercury) were charged with 0.25 mL of stock solution (0.012 M) of catalyst and 0.6 mL of stock solution of diphenylacetylene (0.1 M) in toluene (total volume 0.85 mL). With a microsyringe, 4.2 μL of mesitylene were added to the solution and mixed. Both Schlenks were connected to a gas setup, degassed twice by freeze-pump procedure and H_2 was introduced. Both Schlenk bombs were heated under intense stirring for 5 hours at 70 ºC. After this time, the pressure was released. 0.0062 mmol of dodecane, 5 mL of Et_2O and 1 mL of water were added. The organic phase was extracted, and 1 mL of acetone was added to dilute the mixture. The solution was analyzed by GC-FID and no difference was found in the product concentration.

Experimental procedure for kinetic profiles: Stock solutions of catalyst (0.012 M), (Z)-stilbene and diphenylacetylene (0.1 M) in deuterated toluene were prepared in the glovebox. In a vial, 0.25 mL of catalyst solution and 0.3 mL of each substrate solution as needed were added (semihydrogenation and isomerization profiles volume 0.55 mL; competition catalyst 0.85 mL). With a microsyringe, 4.2 μL of mesitylene were added to the solution and mixed. The reaction mixture was transferred to a J-Young NMR tube. The tube was connected to a gas setup and degassed by two freeze-pump-thaw cycles and with the solution inside of a Dewar with liquid

nitrogen, hydrogen gas was introduced. The solution was warmed up to room temperature and introduced into the NMR spectrometer at either 25 or 70 ºC.

Data analysis for kinetic profiles: Kinetic profiles were monitored by ^{1}H NMR spectroscopy using mesitylene as internal standard. Proton peaks used in quantification (d^8-tol, ppm, 400 MHz):[44]
Diphenylacetylene: 7.46 (m, 4H)
(E)-stilbene: 7.29 (dd, *J*= 8.3, 1.3 Hz, 4H)
(Z)-stilbene: 6.44 (s, 2H)
1,2-diphenylethane: 2.72 (s, 1H)
Mesitylene: 6.67 (s, 3H), 2.13 (s, 9H).
Resting state, complex 4: 2.23 (s, 3H)
Self-hydrogenated catalyst, complex 5: 5.83 (d, 2H) or 2.20 (s, 3H).
Self-hydrogenated catalyst, complex 5': 2.23 (s, 3H).

The aromatic peak of the internal standard (6.67 ppm) was used for quantification in all profiles except for the isomerization at 25 ºC, where the aliphatic peak was used (2.13 ppm). The data was processed with MestReNova program with the data analysis on arrayed spectra. The information was extracted by peak area integration for all kinetic profiles except the catalysis analysis.[75] For the kinetic profiles involving semihydrogenation a background correction was applied on (E)-stilbene by withdrawing the first value of the integration to all the points (to withdraw some intensity corresponding to the resting state). In case of the catalysis analysis in the semihydrogenation profile this was extracted based on the peak height, recommended if peaks of interest have some degree of overlapping.[75] To decrease the effect of noise in the spectra, a background correction was applied on the resting state and self-hydrogenated products. The average of the value of the last 6 points for the resting state was subtracted from all points. In case of the self-hydrogenated products, the average of the value of the first 6 points was subtracted.

X-ray crystal structure determination of self-hydrogenated catalyst (5):[72] $C_{67}H_{58}NiP_2 \cdot C_6H_{14}$, Fw = 1069.95, red needle, 0.39 × 0.06 × 0.06 mm^3, monoclinic, $P2_1/n$ (no. 14), a = 10.2716(6), b = 24.0789(12), c = 46.997(3) Å, β = 92.130(3) °, V = 11615.7(12) Å^3, Z = 8, D_x = 1.224 g/cm^3, μ = 0.43 mm^{-1}. The diffraction experiment was performed on a Bruker Kappa ApexII diffractometer with sealed tube and Triumph monochromator (λ = 0.71073 Å) at a temperature of 150(2) K up to a resolution of $(\sin \theta/\lambda)_{max}$ = 0.57 Å^{-1}. The Eval15 software[76] was used for the intensity integration. The crystal structure is characterized by *pseudo*-translational symmetry (*pseudo*-I centered Bravais lattice). Consequently many reflections are weak or very weak. A numerical absorption correction and scaling was performed with SADABS[77] (correction range 0.84-0.98). A total of 114418 reflections was measured, 18328 reflections were unique (R_{int} = 0.223), 8209 reflections were observed [I>2σ(I)]. The structure was solved with Patterson superposition methods using SHELXT.[78] Structure refinement was performed with SHELXL-2018[79] on F^2 of all reflections. Non-hydrogen atoms were refined freely with anisotropic displacement parameters. The *n*-hexane solvent molecules were refined with a disorder model. The hydrogen atoms of the metal complexes were located in difference Fourier maps, the hydrogen atoms of the solvent were introduced in calculated positions. Hydrogens H71 and H73 were kept fixed at their located position. All other hydrogen atoms were refined with a riding model. 1483 Parameters were refined with 2242 restraints (distances, angles and displacement parameters of all atoms, distances and angles in the disordered *n*-hexane molecules). R1/wR2 [I > 2σ(I)]: 0.0682 / 0.1363.

R1/wR2 [all refl.]: 0.1865 / 0.1793. S = 0.996. Residual electron density between -0.51 and 0.79 e/Å^3. Geometry calculations and checking for higher symmetry was performed with the PLATON program.[80]

Computational methods: DFT calculations were performed using the Gaussian 16 software package version C.01.[81] The tolyl groups in the structure were substituted by phenyl groups for simplicity. Geometry optimizations were carried out in vacuum at the B3LYP-GDB3J/6-31g(d,p) level of theory on all atoms. Frequency analyses on all stationary points were used to ensure that they are minima (no imaginary frequency) or transition states (one imaginary frequency). Transition states were calculated using the QST3 (synchronous transit-guided quasi-Newton number 3) method or using the opt=TS (Berny algorithm) keyword. The guess structure proposed for each TS calculation was based on the results of relaxed potential energy surface scans (PES). ΔG^o was calculated by single point calculation at B3LYP-GDB3J/def2TZVP/SMD(toluene) level of theory adjusting the value with the thermal correction obtained at the B3LYP-GDB3J/6-31g(d,p) level of theory with temperature 298.15 K and pressure 1 atmosphere. QTAIM analysis was perfomed on the single point calculation at B3LYP-GDB3J/def2TZVP/SMD(toluene) level of theory with the Multiwfn program.[60]

Equilibrium under hydrogen gas (^{Ph}bppe^{H,CHptol2})NiH$_2$ (2) and [PCH$_2$CH(p-Tol)$_2$P]NiH (3): [(^{Ph}bppe^{H,CHptol2})Ni]$_2$ (μ-N$_2$) (**1^{dimer}**, 10 mg, 0.006 mmol) was dissolved in 0.5 mL of d^8-toluene and the solution was placed in a J-Young NMR tube. The sample was degassed by two freeze-pump-thaw cycles and, while the tube was immersed in liquid nitrogen, hydrogen gas was introduced. The solution was warmed up to room temperature and analyzed. If the sample is degassed again by two freeze-pump-thaw cycles and nitrogen gas is reintroduced, complex (^{Ph}bppe^{H,CHptol2})NiN$_2$ is regenerated.

Equilibrium mixture at 25 ºC: ^{1}H NMR (400 MHz, d^8-tol, 25 ºC): δ(ppm) δ 7.64 (b, 6H), 7.26 (m, 3H), 7.17 (b, 8H), 6.94–6.84 (m, 10H), 6.79 (b, 9H), 3.84 (s, 1H, C*H*), 2.09 (s, 6H), –14.41 (s, 1H, Ni-*H*). Some peaks are overlapping with the residual solvent signals.

^{31}P{H^1} NMR (162 MHz, d^8-tol, 25 ºC): δ(ppm) 40.1 (s, 2P).

Equilibrium mixture at –40 ºC: ^{1}H NMR (400 MHz, d^8-tol, –40 ºC): δ(ppm) δ 7.84–7.74 (m, 2H), 7.68 (d, *J*= 8.1 Hz, 2H), 7.54 (s, 4H), 7.45 (d, *J*= 7.7 Hz, 1H), 7.38–7.18 (m, 11H), 6.95–6.85 (m, 12H), 6.84–6.73 (m, 11H), 4.76 (s, C*H*$_{olefin}$ complex 1), 4.40 (s, C*H*$_{olefin}$ complex 2), 3.80 (t, $^3J_{H,H}$= 8.4 Hz, 1H, C*H*), 3.12 (b, 2H, C*H*$_2$), -2.09 (b, Ni-*H*$_2$), -14.29 (t, $^2J_{H,P}$= 64.3 Hz, 1H, Ni-*H*).

^{13}C{H^1} NMR (101 MHz, d^8-tol, –40 ºC): δ(ppm) 164.0 (s, Ar), 150.3 (s, Ar), 143.9 (s, Ar), 141.9–140.8 (m, Ar), 139.1 (s, Ar), 138.5–137.6 (m, Ar), 135.1–134.3 (m, Ar), 133.8 (s, Ar), 133.6 (s, Ar), 133.3 (s, Ar), 129.8 (d, *J*= 10.6 Hz), 129.3–129.0 (m, Ar), 125.7 (s, Ar), 125.5 (s, Ar), 65.0 (s, *C*-CH$_2$), 56.9 (s, *C*H$_2$), 50.8 (s, *C*H), 21.3 (s, *C*H$_3$), 21.0 (s, *C*H$_3$).

^{31}P{H^1} NMR (162 MHz, d^8-tol, –40 ºC): δ(ppm) 40.6 (s, 2P), 28.2 (d, $^2J_{P,P}$= 53.3 Hz, 1P), 32.8 (d, $^2J_{P,P}$= 60.2 Hz, 1P), 15.5 (d, $^2J_{P,P}$= 58.7 Hz, 1P), 11.3 (d, $^2J_{P,P}$= 53.6 Hz, 1P).

Characteristic peaks (**2**): ^{1}H NMR (400 MHz, d^8-tol, –40 ºC): δ(ppm) 4.40 (s, 1H, C*H*$_{olefin}$), -2.09 (b, 2H, *H*$_2$)

^{31}P{H^1} NMR (162 MHz, d^8-tol, -40 ºC): δ(ppm) 32.8 (d, $J_{P,P}$= 60.2 Hz, 1P), 15.5 (d, $J_{P,P}$= 58.7 Hz, 1P).

Characteristic peaks (**3**): ^{1}H NMR (400 MHz, d^8-tol, –40 ºC): δ(ppm) 3.80 (t, 1H, C*H*), 3.12 (b, 2H, C*H*$_2$), -14.29 (t, $J_{H,P}$= 64.3 Hz, 1H, Ni-*H*)

^{31}P{H^1} NMR (162 MHz, d^8-tol, –40 ºC): δ(ppm) 40.6 (s, 2P).

^{13}C{H^1} NMR (101 MHz, d^8-tol, –40 ºC): δ(ppm) 56.9 (s, *C*H$_2$), 50.8 (s, *C*H).

Synthesis of [(^{Ph}bppe^{H,CHptol2})Ni(PhCCPh) (4): [(^{Ph}bppe^{H,CHptol2})Ni]$_2$(μ-N$_2$) (**1^{dimer},** 50 mg, 0.030 mmol) was weighted in a vial and dissolved with 5 mL of toluene. Diphenylacetylene (11 mg, 0.062 mmol) dissolved in 1 mL of toluene was added at once and the solution was stirred for 5h. Afterwards, the solution was concentrated to approximately 1 mL under vacuum. Hexane (1 mL) was added to the solution, which was cooled down to –35 ºC for 15 min. The precipitate was separated by decantation, washed with cold hexane twice and dried to obtain the product as a yellow powder (53 mg, 90 % yield). The high sensitivity of the compound did not allow to obtain elemental analysis data.

^{1}H NMR (400 MHz, C$_6$D$_6$, 25 ºC): δ(ppm) 7.52 (dt, *J*=6.9, 1.3 Hz, 2H, Ar-*H*), 7.46–7.40 (m, 2H, Ar-*H*), 7.32–7.25 (m, 3H, Ar-*H*), 7.10 (d, *J*=7.8 Hz, 2H, Ar-*H*), 7.03–6.91 (m, 14H, Ar-*H*), 6.91-6.82 (m, 10H, Ar-*H*), 6.81–6.75 (m, 5H, Ar-*H*), 6.74 (t, *J*=1.5 Hz, 1H, Ar-*H*), 6.69 (td, *J*=7.5, 1.2 Hz, 1H, Ar-*H*), 5.72 (d, *J*=10.5 Hz, 1H, =C*H*R), 4.68 (d, *J*=10.5 Hz, 1H, C*H*p-Tol$_2$), 2.26 (s, 3H, C*H$_3$*), 2.06 (s, 3H, C*H$_3$*).

^{13}C{H^1} NMR (101 MHz, C$_6$D$_6$, 25 ºC): δ(ppm) 150.9 (d, *J*=27.5 Hz, Ar), 143.2 (d, *J*=3.4 Hz, Ar), 141.3 (s, Ar), 139.7 (d, *J*=26.7 Hz, Ar), 138.7 (d, *J*=21.7 Hz, Ar), 137.4 (s, Ar), 137.2 (s, Ar), 137.1 (s, Ar), 136.9 (d, *J*=10.3 Hz, Ar), 136.5 (s, Ar), 136.3 (s, Ar), 136.0 (s, Ar), 135.3 (s, Ar), 135.3 (s, Ar), 135.1 (s, Ar), 134.9 (s, Ar), 133.9 (d, *J*=13.2 Hz, Ar), 133.6 (d, *J*=13.3 Hz, Ar), 133.4–133.1 (m, Ar), 131.9 (s, Ar), 131.2 (d, *J*=9.2 Hz, Ar), 130.6 (d, *J*=10.0 Hz, Ar), 129.4 (d, *J*=15.3 Hz, Ar), 129.1 (s, Ar), 129.0 (s, Ar), 128.8–128.5 (m, Ar), 124.5 (s, Ar or =*C*H) 52.2 (s, *C*Hp-Tol$_2$), 21.1 (s, *C*H$_3$), 21.0 (s, *C*H$_3$).

^{31}P{H^1} NMR (162 MHz, C$_6$D$_6$, 25 ºC): δ(ppm) 27.5 (d, $J_{P,P}$= 38.3 Hz, 1P), 18.4 (b, 1P).

IR (cm^{-1}): 3055, 2954, 2923, 2853, 1679, 1435, 1259, 1094, 1068, 1028, 754, 691, 524.

Synthesis of self-hydrogenated complex (5): [(^{Ph}bppe^{H,CHptol2})Ni]$_2$(μ-N$_2$) (10 mg, 0.006 mmol) were weighted in a vial and dissolved in 0.5 mL of toluene. Diphenylacetylene (11 mg, 0.06 mmol) dissolved in 0.5 mL of toluene was added at once and the solution was mixed. The solution was transferred to a J-Young NMR tube. The tube was connected to a gas setup and degassed by two freeze-pump-thaw cycles and with the solution inside of a Dewar with liquid nitrogen, hydrogen gas was introduced. The solution was warmed up at room temperature and placed in an oil bath at 70 ºC for 16h. After this time, the pressure was released, and the solvent was evaporated. The solid was redissolved in a minimum amount of THF and precipitate with hexane. The precipitate was decantated, washed with cold hexane twice and dried to obtain 8 mg of an orange powder with 70 % yield. Suitable crystals for X-ray diffraction were obtained by vapor diffusion of hexane into a saturated toluene solution. The high sensitivity of the compound did not allow to obtain elemental analysis data.

^{1}H NMR (400 MHz, C$_6$D$_6$, 25 ºC): δ(ppm) 8.52–8.38 (m, 1H, p-tol$_2$CH-CH$_2$-C*H*), 7.80 (d, *J*=7.6 Hz, 2H, Ar-*H)*, 7.75 (t, *J*=8.5 Hz, 2H, Ar-*H*), 7.37 (t, *J*=7.5 Hz, 2H, Ar-*H*), 7.26 (t, *J*=7.2 Hz, 1H, Ar-*H*), 7.22–7.17 (m, 4H, Ar-*H*), 7.15–7.06 (m, 5H, Ar-*H*), 7.06–6.99 (m, 3H, Ar-*H*), 6.95 (dd, *J*=9.3, 5.5 Hz, 2H, Ar-*H*), 6.89 (dd, *J*=10.6, 7.1 Hz, 2H, Ar-*H*), 6.82 (td, *J*=7.6, 4.0 Hz, 5H, Ar-*H*), 6.76 (d, *J*=7.7 Hz, 2H, Ar-*H*), 6.71 (t, *J*=7.7 Hz, 2H, Ar-*H*), 6.63 (dt, *J*=19.9, 7.4 Hz, 3H, Ar-*H*), 6.51 (q, *J*=5.6 Hz, 3H, Ar-*H*), 6.43 (t, *J*=7.5 Hz, 1H, Ar-*H*), 5.83 (d, *J*=7.7 Hz, 2H, Ar-*H*), 5.78 – 5.64 (m, 2H, Ar-*H*), 4.19 (d, *J*=11.3 Hz, 1H, p-tol$_2$C*H*-CH$_2$-CH), 4.16–4.11 (m, 1H, PhC*H*=C), 4.02 (td, *J* = 10.0, 3.5 Hz, 1H, PhC*H*=C), 2.64 (q, *J* = 11.9 Hz, 1H, C*H$_2$*), 2.24 (s, 3H, C*H$_3$*), 2.03 (s, 3H, C*H$_3$*), 1.49 (d, *J*=13.8 Hz, 1H, C*H$_2$*).

^{13}C{H^1} NMR (101 MHz, C$_6$D$_6$, 25 ºC): δ(ppm) 150.5 (d, *J*=18.3 Hz, Ar), 149.0–148.8 (m, Ar), 148.8 (s, Ar), 144.1–143.8 (m, Ar), 143.5 (s, Ar), 142.8 (s, Ar), 138.3 (d, *J*=9.5 Hz, Ar), 138.0 (d, *J*=9.9 Hz, Ar), 137.1 (s, Ar), 136.7 (s, Ar), 136.3 (s, Ar), 136.2 (d, *J*=1.9 Hz, Ar), 135.9 (s, Ar), 135.3 (d, *J*=14.9 Hz, Ar), 135.0 (d, *J*=5.3 Hz, Ar), 134.7 (d, *J*=8.0 Hz, Ar), 134.5 (s, Ar), 134.4 (s, Ar), 134.2 (s, Ar), 133.5 (s, Ar), 133.1 (s, Ar), 133.0 (s, Ar), 132.9 (d, *J*=5.4 Hz, Ar), 132.8 (s, Ar),

130.4 (s, Ar), 130.1 (d, *J*=6.1 Hz, Ar), 129.4 (s, Ar), 129.1 (d, *J*=6.0 Hz, Ar), 128.9 (d, *J*=5.5 Hz, Ar), 128.7 (s, Ar), 128.6 (s, Ar), 128.5 (d, *J*=4.9 Hz, Ar), 127.5 (d, *J*=8.1 Hz, Ar), 127.1 (d, *J*=7.0 Hz, Ar), 126.3 (s, Ar), 125.5 (s, Ar), 124.9 (s, Ar), 124.5 (d, *J*=4.1 Hz, Ar), 123.5 (s, Ar), 122.3 (s, Ar), 65.9 (d, *J*=16.9 Hz, Ph*C*H=C), 61.7 (d, *J*=15.8 Hz, Ph*C*H=C), 51.6 (s, p-tol$_2$*C*H-CH$_2$-CH), 43.8 (dd, *J*=25.8, 12.7 Hz, p-tol$_2$CH-CH$_2$-*C*H), 39.0 (s, *C*H$_2$), 21.1 (d, *J*=2.3 Hz, *C*H$_3$), 20.9 (d, *J*=1.9 Hz, *C*H$_3$).
$^{31}P\{H^1\}$ NMR (162 MHz, C_6D_6, 25 ºC): δ(ppm) 20.16 (d, $J_{P\text{-}P}$= 48 Hz), 17.36 (d, $J_{P\text{-}P}$= 48 Hz).
IR (cm^{-1}): 3055, 2923, 2854, 1588, 1510, 1435, 1262, 1094, 1067, 892, 805, 693, 523.

REFERENCES

1. McGlynn, S. E. *et al.* Hydrogenation reactions of carbon on Earth: Linking methane, margarine, and life. *Am. Mineral.* **105**, 599–608 (2020).
2. Kubas, G. J. Chemistry of Saturated Molecules. *Proc. Natl. Acad. Sci. U. S. A.* **104**, 6901–6907 (2007).
3. Kubas, G. J. Catalytic processes involving dihydrogen complexes and other sigma-bond complexes. *Catal. Letters* **104**, 79–101 (2005).
4. Crabtree, R. H. Dihydrogen Complexation. *Chem. Rev.* **116**, 8750–8769 (2016).
5. Hale, D. J., Ferguson, M. J. & Turculet, L. (PSiP)Ni-Catalyzed (E)-Selective Semihydrogenation of Alkynes with Molecular Hydrogen. *ACS Catal.* 146–155 (2021). doi:10.1021/acscatal.1c04537
6. Kubas, G. J. Activation of dihydrogen and coordination of molecular H2 on transition metals. *J. Organomet. Chem.* **751**, 33–49 (2014).
7. Kubas, G. J. Metal-dihydrogen and σ-bond coordination: The consummate extension of the Dewar-Chatt-Duncanson model for metal-olefin π bonding. *J. Organomet. Chem.* **635**, 37–68 (2001).
8. Kubas, G. J. Fundamentals of H 2 binding and reactivity on transition metals underlying hydrogenase function and H 2 production and storage. *Chem. Rev.* **107**, 4152–4205 (2007).
9. Vollmer, M. V., Xie, J. & Lu, C. C. Stable Dihydrogen Complexes of Cobalt(-I) Suggest an Inverse trans-Influence of Lewis Acidic Group 13 Metalloligands. *J. Am. Chem. Soc.* **139**, 6570–6573 (2017).
10. Jessop, P. G. & Morris, R. H. Reactions of transition metal dihydrogen complexes. *Coord. Chem. Rev.* **121**, 155–284 (1992).
11. Alig, L., Fritz, M. & Schneider, S. First-Row Transition Metal (De)Hydrogenation Catalysis Based on Functional Pincer Ligands. *Chem. Rev.* **119**, 2681–2751 (2019).
12. Manar, K. K. & Ren, P. *Recent progress on group 10 metal complexes of pincer ligands: From synthesis to activities and catalysis*. *Advances in Organometallic Chemistry* **76**, (Elsevier Inc., 2021).
13. Karunananda, M. K. & Mankad, N. P. Cooperative Strategies for Catalytic Hydrogenation of Unsaturated Hydrocarbons. *ACS Catal.* **7**, 6110–6119 (2017).
14. Grotjahn, D. B. Bifunctional organometallic catalysts involving proton transfer or hydrogen bonding. *Chem. - A Eur. J.* **11**, 7146–7153 (2005).
15. Tiddens, M. R. & Moret, M.-E. Metal-Ligand Cooperation at Phosphine-Based Acceptor Pincer Ligands. in (2020). doi:10.1007/3418_2020_70
16. Elsby, M. R. & Baker, R. T. Strategies and mechanisms of metal-ligand cooperativity in first-row transition metal complex catalysts. *Chem. Soc. Rev.* **49**, 8933–8987 (2020).
17. Milstein, D. Metal–ligand cooperation by aromatization–dearomatization as a tool in

single bond activation. *Philos. Trans. R. Soc. A Math. Phys. Eng. Sci.* **373**, 20140189 (2015).
18. Van Der Vlugt, J. I. Cooperative catalysis with first-row late transition metals. *Eur. J. Inorg. Chem.* 363–375 (2012). doi:10.1002/ejic.201100752
19. Grützmacher, H. Cooperating Ligands in Catalysis. *Angew. Chemie Int. Ed.* **47**, 1814–1818 (2008).
20. He, T. *et al.* Mechanism of heterolysis of H2 by an Unsaturated d8 nickel center: Via tetravalent nickel? *J. Am. Chem. Soc.* **132**, 910–911 (2010).
21. Schneider, S., Meiners, J. & Askevold, B. Cooperative aliphatic PNP amido pincer ligands-versatile building blocks for coordination chemistry and catalysis. *Eur. J. Inorg. Chem.* 412–429 (2012). doi:10.1002/ejic.201100880
22. Harman, W. H. & Peters, J. C. Reversible H 2 addition across a nickel-borane unit as a promising strategy for catalysis. *J. Am. Chem. Soc.* **134**, 5080–5082 (2012).
23. Harman, W. H., Lin, T. P. & Peters, J. C. A d10 Ni-(H2) adduct as an intermediate in H-H oxidative addition across a Ni-B bond. *Angew. Chemie - Int. Ed.* **53**, 1081–1086 (2014).
24. Karunananda, M. K. & Mankad, N. P. E-Selective Semi-Hydrogenation of Alkynes by Heterobimetallic Catalysis. *J. Am. Chem. Soc.* **137**, 14598–14601 (2015).
25. Kubas, G. J., Ryan, R. R., Swanson, B. I., Vergamini, P. J. & Wasserman, H. J. Characterization of the First Examples of Isolable Molecular Hydrogen Complexes, M(CO)3(PR3)2(H2). *J. Am. Chem. Soc.* **106**, 451–452 (1984).
26. Bianchini, C. *et al.* Selective Hydrogenation of 1-Alkynes to Alkenes Catalyzed by an Iron(II) cis-Hydride η2-Dihydrogen Complex. A Case of Intramolecular Reaction between η2-H2 and-σ-Vinyl Ligands. *Organometallics* **11**, 138–145 (1992).
27. Thomas, A., Haake, M., Grevels, F. -W & Bargon, J. In Situ NMR Investigations of Photocatalyzed Hydrogenations with Parahydrogen in the Presence of Metal Carbonyl Compounds of Group 6. *Angew. Chemie Int. Ed. English* **33**, 755–757 (1994).
28. Joshi, A. M., MacFarlane, K. S. & James, B. R. Kinetics and mechanism of H2-hydrogenation of styrene catalyzed by [RuCl(dppb) (μ-Cl)]2 (dppb = 1,4-bis(dipphenylphosphino)butane). Evidence for hydrogen transfer from a dinuclear molecular hydrogen species. *J. Organomet. Chem.* **488**, 161–167 (1995).
29. Kirss, R. U., Eisenschmid, T. C. & Eisenberg, R. Para Hydrogen Induced Polarization in Hydrogenation Reactions Catalyzed by Ruthenium-Phosphine Complexes. *J. Am. Chem. Soc.* **110**, 8564–8566 (1988).
30. Jia, G., Ng, W. S. & Lau, C. P. Dihydrogen complex formation and C-C bond cleavage from protonation of Cp*RuH(diene) complexes. *Organometallics* **17**, 4538–4540 (1998).
31. Kubas, G. J. *Metal Dihydrogen and σ-Bond Complexes*. (Springer US, 2001). doi:10.1007/b113929
32. Vigalok, A., Kraatz, H., Konstantinovsky, L. & Milstein, D. Evidence for direct trans insertion in a hydrido-olefin rhodium complex - Free nitrogen as a trap in a migratory insertion process. *Chem. - A Eur. J.* **3**, 253–260 (1997).
33. Polukeev, A. V. & Wendt, O. F. Iridium Pincer Complexes with an Olefin Backbone. *Organometallics* **34**, 4262–4271 (2015).
34. Polukeev, A. V. & Wendt, O. F. Iridium complexes with aliphatic, non-innocent pincer ligands. *J. Organomet. Chem.* **867**, 33–50 (2018).
35. Verhoeven, D. G. A. & Moret, M. E. Metal-ligand cooperation at tethered π-ligands. *Dalt. Trans.* **45**, 15762–15778 (2016).
36. Comanescu, C. C., Vyushkova, M. & Iluc, V. M. Palladium carbene complexes as persistent radicals. *Chem. Sci.* **6**, 4570–4579 (2015).
37. Barrett, B. J. & Iluc, V. M. An Adaptable Chelating Diphosphine Ligand for the

Stabilization of Palladium and Platinum Carbenes. *Organometallics* **36**, 730–741 (2017).
38. Barrett, B. J. & Iluc, V. M. Group 10 metal complexes supported by pincer ligands with an olefinic backbone. *Organometallics* **33**, 2565–2574 (2014).
39. Barrett, B. J. & Iluc, V. M. Coordination of a hemilabile pincer ligand with an olefinic backbone to mid-to-late transition metals. *Inorg. Chem.* **53**, 7248–7259 (2014).
40. Breitenfeld, J., Vechorkin, O., Corminboeuf, C., Scopelliti, R. & Hu, X. Why are (NN2)Ni pincer complexes active for alkyl-alkyl coupling: β-H elimination is kinetically accessible but thermodynamically uphill. *Organometallics* **29**, 3686–3689 (2010).
41. Crabtree, R. H. *The Organometallic Chemistry of the Transition Metals*. (John Wiley & Sons, Inc., 2014). doi:10.1002/9781118788301
42. Michaliszyn, K., Smirnova, E. S., Bucci, A., Martin-Diaconescu, V. & Lloret Fillol, J. Well-defined Nickel P 3 C Complexes as Hydrogenation Catalysts of N -Heteroarenes Under Mild Conditions. *ChemCatChem* **14**, 0–3 (2022).
43. Murugesan, K. *et al.* Nickel-Catalyzed Stereodivergent Synthesis of E- and Z-Alkenes by Hydrogenation of Alkynes. *ChemSusChem* **12**, 3363–3369 (2019).
44. Ramirez, B. L. & Lu, C. C. Rare-Earth Supported Nickel Catalysts for Alkyne Semihydrogenation: Chemo- And Regioselectivity Impacted by the Lewis Acidity and Size of the Support. *J. Am. Chem. Soc.* **142**, 5396–5407 (2020).
45. Thiel, N. O., Kaewmee, B., Tran Ngoc, T. & Teichert, J. F. A Simple Nickel Catalyst Enabling an E-Selective Alkyne Semihydrogenation. *Chem. - A Eur. J.* **26**, 1597–1603 (2020).
46. Swamy, K. C. K., Reddy, A. S., Sandeep, K. & Kalyani, A. Advances in chemoselective and/or stereoselective semihydrogenation of alkynes. *Tetrahedron Lett.* **59**, 419–429 (2018).
47. Gregori, B. J., Jacobi von Wangelin, A. & Schmotz, M.-O. W. S. Stereoselective Semi-Hydrogenations of Alkynes by First-Row (3d) Transition Metal Catalysts. *ChemCatChem* (2022). doi:10.1002/cctc.202200886
48. Sansores-Paredes, M. L. G., Voort, S., Lutz, M. & Moret, M. Divergent Reactivity of an Isolable Nickelacyclobutane. *Angew. Chemie Int. Ed.* **60**, 26518–26522 (2021).
49. Gullett, K. L. *et al. Dihydrogen and Dinitrogen Complexes of Cobalt and Nickel*. *Comprehensive Coordination Chemistry III* **6**, (Elsevier, 2021).
50. Morris, R. H. Dihydrogen, dihydride and in between: NMR and structural properties of iron group complexes. *Coord. Chem. Rev.* **252**, 2381–2394 (2008).
51. Luther, T. A. & Heinekey, D. M. Synthesis, Characterization, and Reactivity of Dicationic Dihydrogen Complexes of Osmium and Ruthenium. *Inorg. Chem.* **37**, 127–132 (1998).
52. Cammarota, R. C. & Lu, C. C. Tuning Nickel with Lewis Acidic Group 13 Metalloligands for Catalytic Olefin Hydrogenation. *J. Am. Chem. Soc.* **137**, 12486–12489 (2015).
53. Cammarota, R. C. *et al.* Thermodynamic and kinetic studies of H2 and N2 binding to bimetallic nickel-group 13 complexes and neutron structure of a Ni(η2-H2) adduct. *Chem. Sci.* **10**, 7029–7042 (2019).
54. Connor, B. A., Rittle, J., Vandervelde, D. & Peters, J. C. A Ni0(η2-(Si-H))(η2-H2) Complex That Mediates Facile H Atom Exchange between Two σ-Ligands. *Organometallics* **35**, 686–690 (2016).
55. Tsay, C. & Peters, J. C. Thermally stable N2 and H2 adducts of cationic nickel(II). *Chem. Sci.* **3**, 1313–1318 (2012).
56. Connelly, S. J., Zimmerman, A. C., Kaminsky, W. & Heinekey, D. M. Synthesis, structure, and reactivity of a nickel dihydrogen complex. *Chem. - A Eur. J.* **18**, 15932–15934 (2012).
57. Robinson, S. J. C. & Heinekey, D. M. Hydride & dihydrogen complexes of earth abundant metals: structure, reactivity, and applications to catalysis. *Chem. Commun.* **53**, 669–676

(2017).
58. Prat, J. R., Cammarota, R. C., Graziano, B. J., Moore, J. T. & Lu, C. C. Toggling the Z-type interaction off-on in nickel-boron dihydrogen and anionic hydride complexes. *Chem. Commun.* **58**, 8798–8801 (2022).
59. Cammarota, R. C. *et al.* A Bimetallic Nickel-Gallium Complex Catalyzes CO2 Hydrogenation via the Intermediacy of an Anionic d10 Nickel Hydride. *J. Am. Chem. Soc.* **139**, 14244–14250 (2017).
60. Lu, T. & Chen, F. Multiwfn: A multifunctional wavefunction analyzer. *J. Comput. Chem.* **33**, 580–592 (2012).
61. Vastine, B. A. & Hall, M. B. Carbon-hydrogen bond activation: Two, three, or more mechanisms? *J. Am. Chem. Soc.* **129**, 12068–12069 (2007).
62. Skipper, C. V. J., Hoang, T. K. A., Antonelli, D. M. & Kaltsoyannis, N. Transition metal hydrazide-based hydrogen-storage materials: The first atoms-in-molecules analysis of the Kubas interaction. *Chem. - A Eur. J.* **18**, 1750–1760 (2012).
63. Sparkes, H. A., Chaplin, A. B., Weller, A. S. & Howard, J. A. K. Bond catastrophes in rhodium complexes: Experimental charge-density studies of [Rh(C7H8)(PtBu3)Cl] and [Rh(C7H8)(PCy3)Cl]. *Acta Crystallogr. Sect. B Struct. Sci.* **66**, 503–514 (2010).
64. Guihaumé, J., Halbert, S., Eisenstein, O. & Perutz, R. N. Hydrofluoroarylation of alkynes with Ni catalysts. C-H activation via ligand-to-ligand hydrogen transfer, an alternative to oxidative addition. *Organometallics* **31**, 1300–1314 (2012).
65. Perutz, R. N., Sabo-Etienne, S. & Weller, A. S. Metathesis by Partner Interchange in σ-Bond Ligands: Expanding Applications of the σ-CAM Mechanism. *Angew. Chemie - Int. Ed.* 2–24 (2021). doi:10.1002/anie.202111462
66. Tang, S., Eisenstein, O., Nakao, Y. & Sakaki, S. Aromatic C-H σ-Bond Activation by Ni0, Pd0, and Pt0 Alkene Complexes: Concerted Oxidative Addition to Metal vs Ligand-to-Ligand H Transfer Mechanism. *Organometallics* **36**, 2761–2771 (2017).
67. Perutz, R. N. & Sabo-Etienne, S. The σ-CAM mechanism: σ complexes as the basis of σ-bond metathesis at late-transition-metal centers. *Angew. Chemie - Int. Ed.* **46**, 2578–2592 (2007).
68. Bair, J. S. *et al.* Linear-selective hydroarylation of unactivated terminal and internal olefins with trifluoromethyl-substituted arenes. *J. Am. Chem. Soc.* **136**, 13098–13101 (2014).
69. Chen, M. & Montgomery, J. Nickel-Catalyzed Intermolecular Enantioselective Heteroaromatic C–H Alkylation. *ACS Catal.* 11015–11023 (2022). doi:10.1021/acscatal.2c03228
70. Saper, N. I. *et al.* Nickel-catalysed anti-Markovnikov hydroarylation of unactivated alkenes with unactivated arenes facilitated by non-covalent interactions. *Nat. Chem.* **12**, 276–283 (2020).
71. Orsino, A. F., Gutiérrez Del Campo, M., Lutz, M. & Moret, M. E. Enhanced Catalytic Activity of Nickel Complexes of an Adaptive Diphosphine-Benzophenone Ligand in Alkyne Cyclotrimerization. *ACS Catal.* **9**, 2458–2481 (2019).
72. CCDC 2236144 contains the supplementary crystallographic data for this paper. These data can be obtained free of charge from The Cambridge Crystallographic Data Centre via www.ccdc.cam.ac.uk/data_request/cif.
73. Lesueur, W., Solari, E., Floriani, C., Chiesi-Villa, A. & Rizzoli, C. A Bidentate Bisphosphine Functioning in Intramolecular Aliphatic Metalation and as an NMR Spectroscopic Probe for the Metal Coordination Environment. *Inorg. Chem.* **36**, 3354–3362 (1997).
74. Ryu, H. *et al.* Pitfalls in Computational Modeling of Chemical Reactions and How to Avoid Them. *Organometallics* **37**, 3228–3239 (2018).

75. Basics on Arrayed-NMR and Data Analysis. https://resources.mestrelab.com/data-analysis/ (Consulted in January 2023)
76. Schreurs, A. M. M.; Xian, X.; Kroon-Batenburg, L. M. J. EVAL15: A Diffraction Data Integration Method Based on Ab Initio Predicted Profiles. *J. Appl. Crystallogr.* **2010**, *43* (1), 70–82. https://doi.org/10.1107/S0021889809043234.
77. Krause, L.; Herbst-Irmer, R.; Sheldrick, G. M.; Stalke, D. Comparison of Silver and Molybdenum Microfocus X-Ray Sources for Single-Crystal Structure Determination. *J. Appl. Crystallogr.* **2015**, *48* (1), 3–10. https://doi.org/10.1107/S1600576714022985.
78. Sheldrick, G. M. SHELXT - Integrated Space-Group and Crystal-Structure Determination. *Acta Crystallogr. Sect. A Found. Crystallogr.* **2015**, *71* (1), 3–8. https://doi.org/10.1107/S2053273314026370.
79. Sheldrick, G. M. Crystal Structure Refinement with SHELXL. *Acta Crystallogr. Sect. C Struct. Chem.* **2015**, *71* (Md), 3–8. https://doi.org/10.1107/S2053229614024218.
80. Spek, A. L. Structure Validation in Chemical Crystallography. *Acta Crystallogr. Sect. D Biol. Crystallogr.* **2009**, *65* (2), 148–155. https://doi.org/10.1107/S090744490804362X.
81. Frisch, M. J.; Trucks, G. W.; Schlegel, H. B.; Scuseria, G. E.; Robb, M. a.; Cheeseman, J. R.; Scalmani, G.; Barone, V.; Petersson, G. a.; Nakatsuji, H.; et al. G16_C01. 2016, p Gaussian 16, Revision C.01, Gaussian, Inc., Wallin.